Science Advances
AAAS

# Supplementary Materials for

## Multiplexed high-throughput immune cell imaging reveals molecular health-associated phenotypes

Yannik Severin *et al.*

Corresponding author: Berend Snijder, snijder@imsb.biol.ethz.ch

*Sci. Adv.* **8**, eabn5631 (2022)
DOI: 10.1126/sciadv.abn5631

**The PDF file includes:**



**Other Supplementary Material for this manuscript includes the following:**

Fig. S1

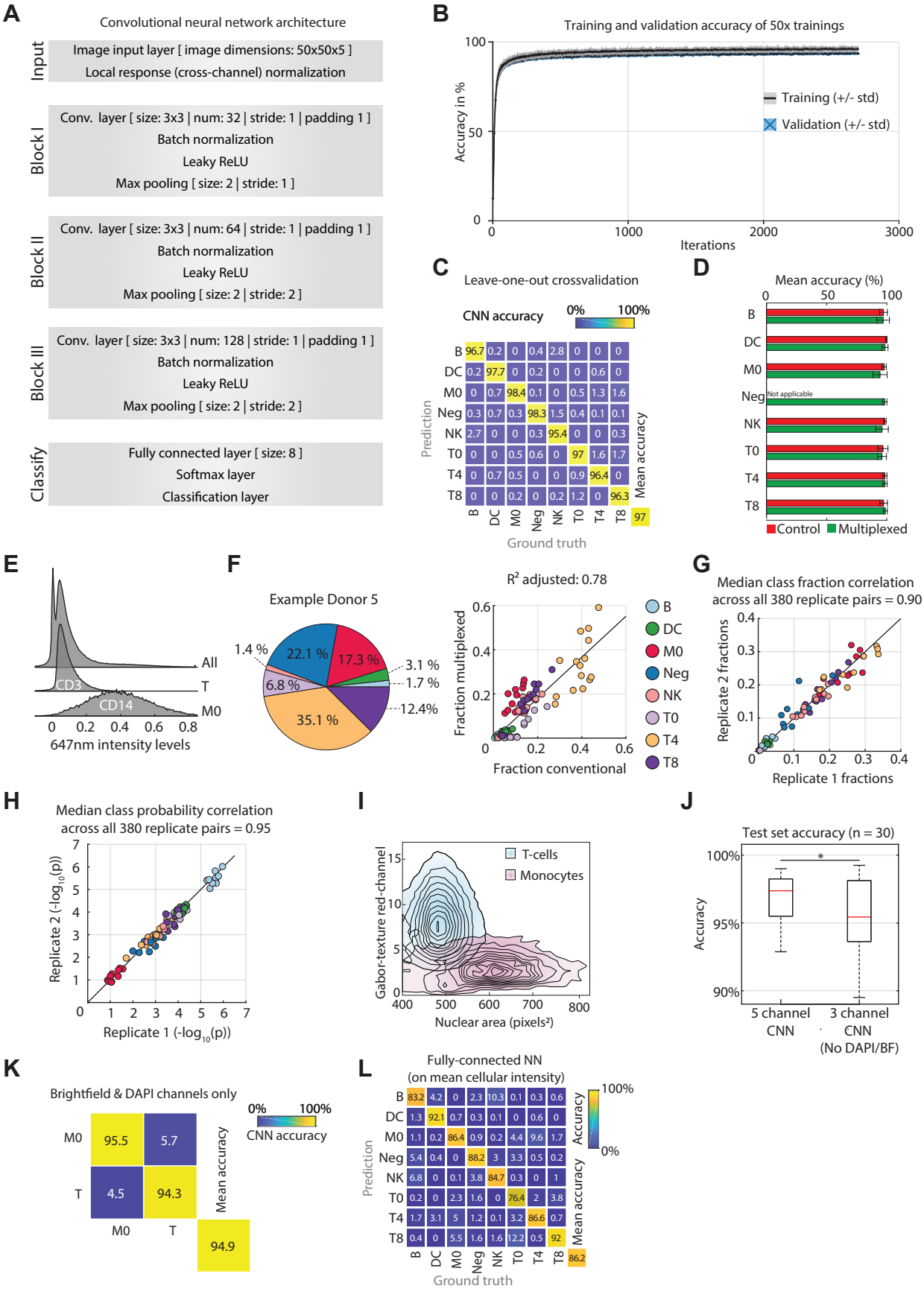
A
Convolutional neural network architecture
Input
Image input layer [ image dimensions: 50x50x5 ]
Local response (cross-channel) normalization
Block I
Conv. layer [ size: 3x3 | num: 32 | stride: 1 | padding 1 ]
Batch normalization
Leaky ReLU
Max pooling [ size: 2 | stride: 1 ]
Block II
Conv. layer [ size: 3x3 | num: 64 | stride: 1 | padding 1 ]
Batch normalization
Leaky ReLU
Max pooling [ size: 2 | stride: 2 ]
Block III
Conv. layer [ size: 3x3 | num: 128 | stride: 1 | padding 1 ]
Batch normalization
Leaky ReLU
Max pooling [ size: 2 | stride: 2 ]
Classify
Fully connected layer [ size: 8 ]
Softmax layer
Classification layer
B
Training and validation accuracy of 50x trainings
Accuracy in %
Iterations
Training (+/- std)
Validation (+/- std)
C
Leave-one-out crossvalidation
CNN accuracy
0%
100%
Prediction
Mean accuracy
Ground truth
D
Mean accuracy (%)
Not applicable
Control
Multiplexed
E
All
T
M0
CD3
CD14
647nm intensity levels
F
Example Donor 5
22.1 %
17.3 %
1.4 %
3.1 %
1.7 %
6.8 %
12.4%
35.1 %
R² adjusted: 0.78
Fraction multiplexed
Fraction conventional
G
Median class fraction correlation
across all 380 replicate pairs = 0.90
Replicate 2 fractions
Replicate 1 fractions
H
Median class probability correlation
across all 380 replicate pairs = 0.95
Replicate 2 (-log10(p))
Replicate 1 (-log10(p))
I
T-cells
Monocytes
Gabor-texture red-channel
Nuclear area (pixels²)
J
Test set accuracy (n = 30)
Accuracy
5 channel CNN
3 channel CNN (No DAPI/BF)
K
Brightfield & DAPI channels only
95.5
5.7
4.5
94.3
94.9
CNN accuracy
L
Fully-connected NN
(on mean cellular intensity)
Prediction
Accuracy
Mean accuracy
Ground truth

**Figure S1. Training and validation of the deep learning-enabled multiplexed PBMC imaging workflow**

**(A)** Overview of the convolutional neural network architecture. **(B)** Average and standard deviation of training and validation accuracies over 20 randomly initialized CNN instances. Validation set represents 10% of the initial training set (n=8948). Network training after 20 epoches. **(C)** Confusion matrix of CNN performance on a leave-one-out cross validation per donor. The CNN was trained with 14 donors and subsequently tested on an unseen donor not included in the training dataset. The confusion matrix shows the mean accuracies after iterating across all donors. **(D)** Comparison of prediction accuracy on conventionally stained and multiplexed cells. Bar plots show the mean accuracy (in %) and the standard deviation of the CNN prediction across all donors individually per class and staining. **(E)** Distribution of 647nm intensity levels across all cells (upper), classified $CD3^+$ T-cells (middle) and classified $CD14^+$ monocytes (lowest) of Donor 1. A cell class probability threshold of 0.8 was applied. **(F)** Population percentages for Donor 5 (left) and class fraction comparison of conventionally stained and multiplexed cells across 15 healthy donors. Negative cell class is excluded due to its unavailability in conventional stainings. **(G)** Class fraction comparison of two single replicates (plate wells) across all 10 donors. Each dot corresponds to a replicate pair from a single donor. Color indicates the cell type. The median pairwise correlation across all technical replicates is indicated. **(H)** Median class probability comparison of two single replicates (plate wells) across all 15 donors. Shown statistic depicts the median class probability correlation of all pairwise replicate combinations per donor across two individual 384 well plates. **(I)** Comparison of selected morphological and staining-pattern parameters divergent between T-cells and monocytes. Conventionally stained T-cells and monocytes from Donor 1 were identified by immunofluorescence gating for CD3 and CD14, respectively. Morphological features were extracted by CellProfiler. **(J)** Test set accuracies of either a CNN trained on all 5 channels, or trained without the DAPI & BF channel. Boxplots show the accuracies of the multiplexed and control test-sets of each of the 15 donors; n=30. **(K)** Confusion matrix of CNN performance on classifying T-cells and monocytes based on brightfield and DAPI channels only. An adapted CNN architecture (2-channel input and 2 class output) was trained with 1900 2-channel images of T-cells and monocytes. Network performance was evaluated in the curated test set containing 750 cells per class. **(L)** Confusion matrix of the performance of a feedforward fully-connected neural network with a size of 10 nodes trained on mean channel intensity measurements. Mean intensity features per single-cell were measured using CellProfiler for all five channels, matching the cells used in the CNN training and test sets.

Fig. S2

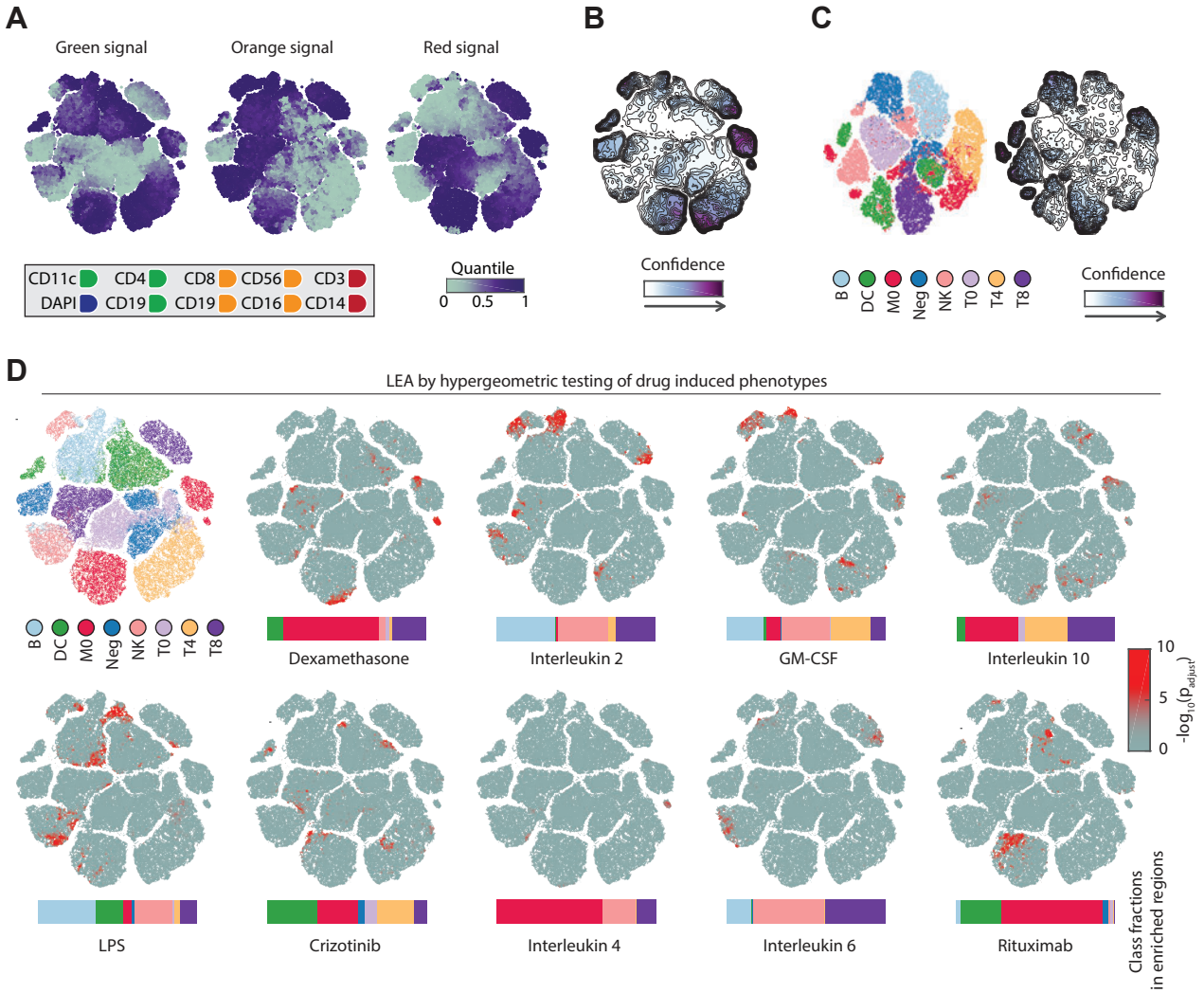
A
Green signal
Orange signal
Red signal
CD11c CD4 CD8 CD56 CD3
DAPI CD19 CD19 CD16 CD14
Quantile
0 0.5 1
B
Confidence
C
B DC M0 Neg NK T0 T4 T8
Confidence
D
LEA by hypergeometric testing of drug induced phenotypes
B DC M0 Neg NK T0 T4 T8
Dexamethasone
Interleukin 2
GM-CSF
Interleukin 10
LPS
Crizotinib
Interleukin 4
Interleukin 6
Rituximab
10
5
0
-log10(padjust)
Class fractions
in enriched regions

**Figure S2. Detailed view on the perturbed immune system of a single donor.**

**(A)** Selected single-cell features mapped onto the same t-SNE map as depicted in Figure 3A. Median value of overlapping data points is calculated and color is assigned accordingly. Points are plotted in order of intensity, from highest to lowest. **(B)** Associated CNN probability contour plot of the phenotypic landscape of the immune system depicted in Figure 3A. **(C)** Left: Phenotypic landscape of the immune system across ten healthy donors. t-SNE embedding of the 8-class CNN probabilities without a confidence threshold of up to 1000 randomly subsampled multiplexed cells per class and per donor. Right: Associated CNN probability contour plot of the phenotypic landscape depicted left. **(D)** LEAs visualized by t-SNE of drug induced phenotypes. Horizontal bar graphs indicate the class fractions in enriched regions (at $p_{adjust} < 0.01$).

Fig. S3

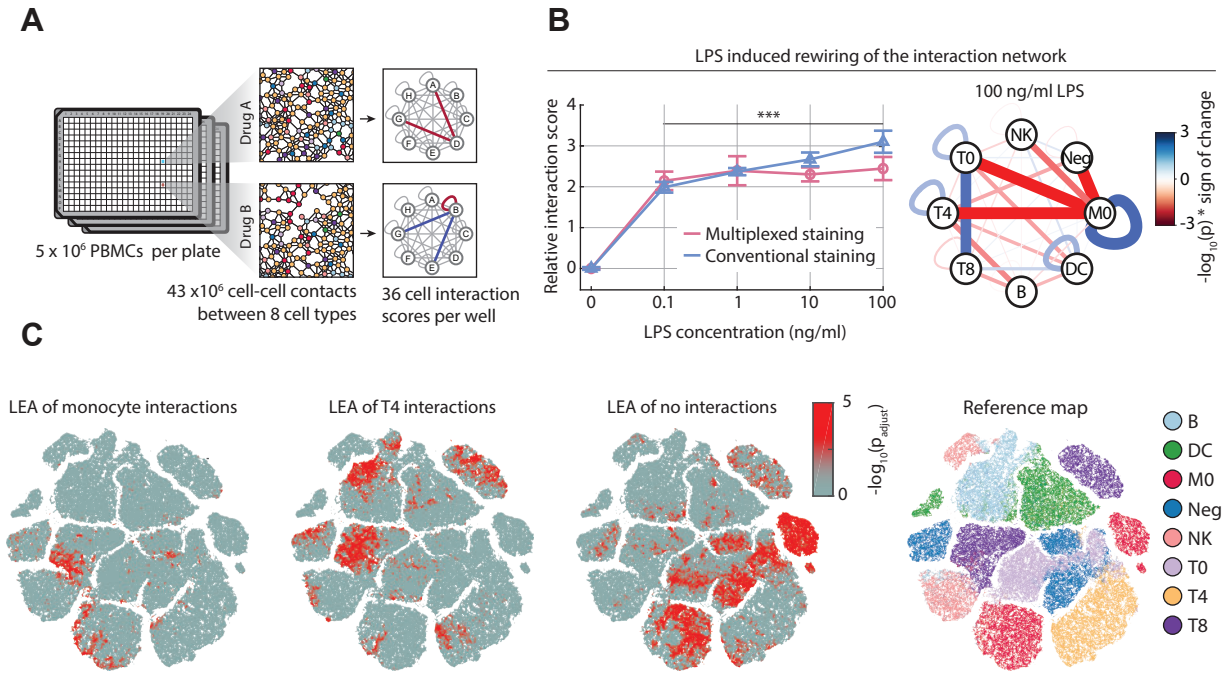
A
Drug A
Drug B
5 x 10⁶ PBMCs per plate
43 x10⁶ cell-cell contacts between 8 cell types
36 cell interaction scores per well
B
LPS induced rewiring of the interaction network
Relative interaction score
***
Multiplexed staining
Conventional staining
LPS concentration (ng/ml)
100 ng/ml LPS
NK
Neg
T0
T4
M0
T8
DC
B
-log10(p)* sign of change
C
LEA of monocyte interactions
LEA of T4 interactions
LEA of no interactions
-log10(padjust)
Reference map
B
DC
M0
Neg
NK
T0
T4
T8

**Figure S3. Perturbation-induced rewiring of cell-cell contacts of the human immune system.**

**(A)** Overview of cell-cell contact analysis over five million PBMCs. Cell-to-cell interaction networks between eight different immune cell populations with a total of 36 cell type interactions were generated per well, and compared across conditions. **(B)** LPS-induced rewiring of the cell-to-cell interaction network. Relative monocyte-to-monocyte interaction scores of multiplexed and conventionally stained wells as a function of increasing LPS concentration (left). Mean interaction score across all replicates is calculated and normalized against control treatment. Example LPS interaction network for 100ng/ml LPS (right). Significance of interaction ($-\log_{10}(p)$, multiplied times the sign of the phenotype (either positive or negative interaction score)). **(C)** LEA of cells with monocytes (left), T-cells (middle) or no-nearest neighbor (right).

Fig. S4

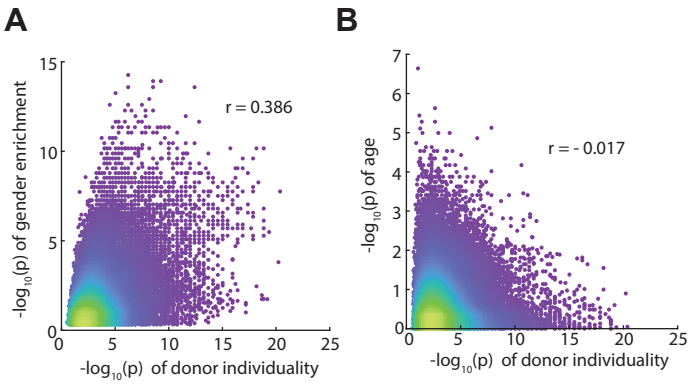
A
B
r = 0.386
r = - 0.017
-log10(p) of gender enrichment
-log10(p) of age
-log10(p) of donor individuality
-log10(p) of donor individuality

**Figure S4. Comparative analysis of LEA-based phenotype and health parameter associations**

**(A)** Comparison of donor LEA enrichments (as in Figure 4A) vs gender LEA enrichments (as in Figure 4B) per single cell. r values represent Pearson correlations. **(B)** Comparison of donor LEA enrichments vs age LEA enrichments per single cell (as in Figure 4D). R values represent pearson correlations.

Fig. S5

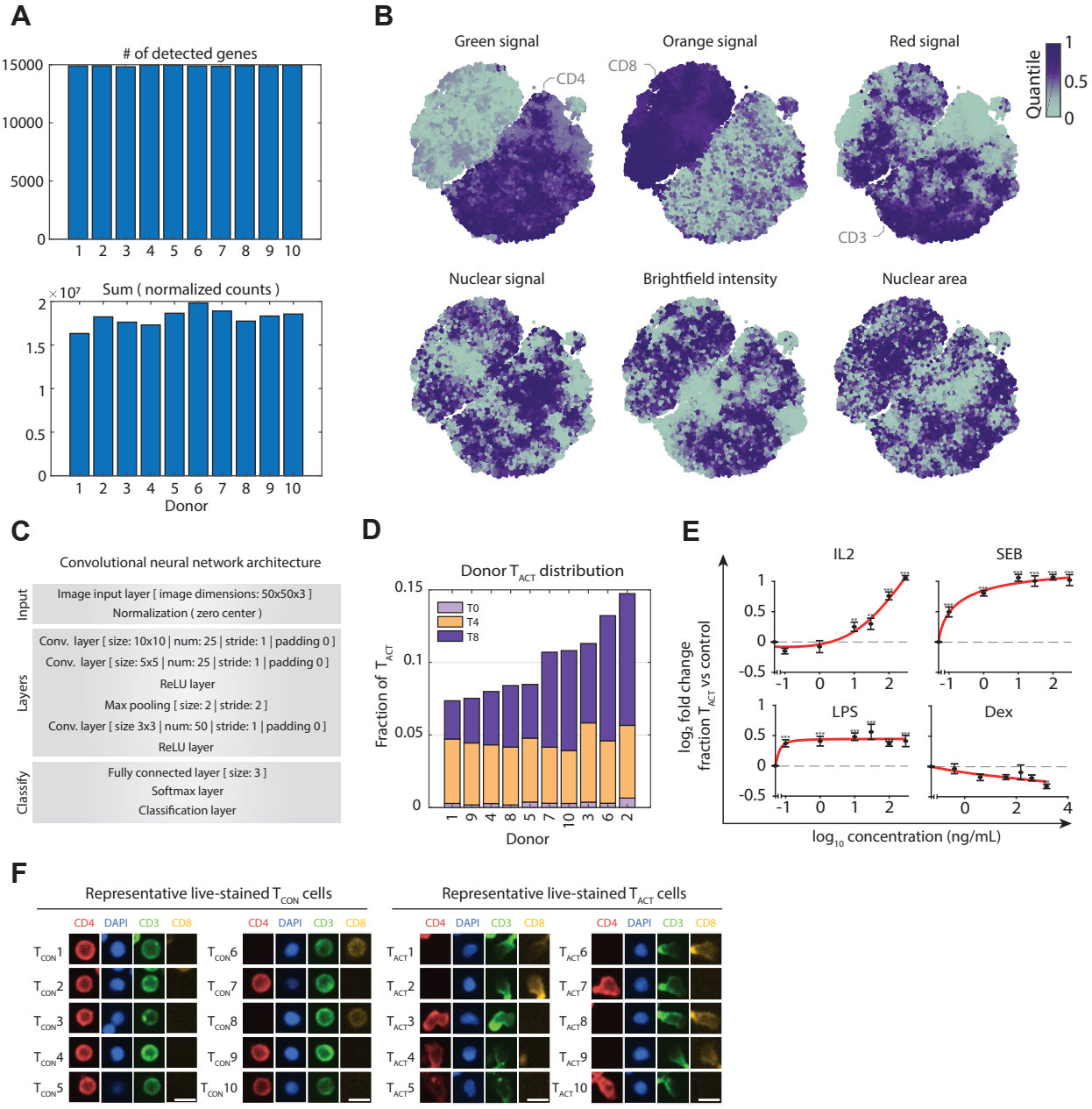
A
# of detected genes
15000
10000
5000
0
1 2 3 4 5 6 7 8 9 10
Sum ( normalized counts )
×10⁷
2
1.5
1
0.5
0
1 2 3 4 5 6 7 8 9 10
Donor
B
Green signal
Orange signal
Red signal
CD4
CD8
CD3
Quantile
1
0.5
0
Nuclear signal
Brightfield intensity
Nuclear area
C
Convolutional neural network architecture
Input
Image input layer [ image dimensions: 50x50x3 ]
Normalization ( zero center )
Layers
Conv. layer [ size: 10x10 | num: 25 | stride: 1 | padding 0 ]
Conv. layer [ size: 5x5 | num: 25 | stride: 1 | padding 0 ]
ReLU layer
Max pooling [ size: 2 | stride: 2 ]
Conv. layer [ size 3x3 | num: 50 | stride: 1 | padding 0 ]
ReLU layer
Classify
Fully connected layer [ size: 3 ]
Softmax layer
Classification layer
D
Donor T_ACT distribution
Fraction of T_ACT
0.15
0.1
0.05
0
T0
T4
T8
1 9 4 8 5 7 10 3 6 2
Donor
E
IL2
SEB
LPS
Dex
log2 fold change fraction T_ACT vs control
log10 concentration (ng/mL)
F
Representative live-stained T_CON cells
Representative live-stained T_ACT cells
CD4 DAPI CD3 CD8
T_CON1
T_CON2
T_CON3
T_CON4
T_CON5
T_CON6
T_CON7
T_CON8
T_CON9
T_CON10
T_ACT1
T_ACT2
T_ACT3
T_ACT4
T_ACT5
T_ACT6
T_ACT7
T_ACT8
T_ACT9
T_ACT10

**Figure S5. T-cell transcriptomics, phenotyping, and validation of an activated T-cell morphology.**

**(A)** Upper: Bar graphs indicate the number of detected transcripts (protein coding and long non-coding RNAs) after applying a threshold of 20 raw counts. Lower: Bar graphs indicated the sum of transcript counts after DESeq2 normalization (*76*). **(B)** Selected single-cell features projected onto the t-SNE depicted in Figure 5A. Median value of overlapping data points is calculated and color is assigned accordingly. Points are plotted in ascending order with the lowest intensity on top. **(C)** Overview of the label-free T-cell activation ($T_{ACT}$) convolutional neural network architecture. **(D)** Fraction of $T_{ACT}$ cells per class and per donor. Stacked bar plots show the mean fraction of all T-cells per donor classified as $T_{ACT}$, within their respective T-cell subclass (T0, T4 or T8) in control (DMSO) conditions. **(E)** Induction and suppression of the $T_{ACT}$ cell phenotype by immunomodulatory agents. Plotted are the $\log_2$ fold changes of the mean fraction of T-cells classified as $T_{ACT}$ across all wells of each drug condition compared to control treatments. Cells were incubated with immunomodulatory agents at 0.1, 1, 10, 30, 100 and 300 ng/ml. Error bars show the standard error of the mean across wells for each drug condition. A custom Hill function (adjusted to different minima and maxima) was used to fit the data (red line). **(E)** Representative live-stained $T_{ACT}$ and $T_{CON}$ cell morphologies. Crop-size is 15 x 15 µm. All scale bars = 10µm.

Fig. S6

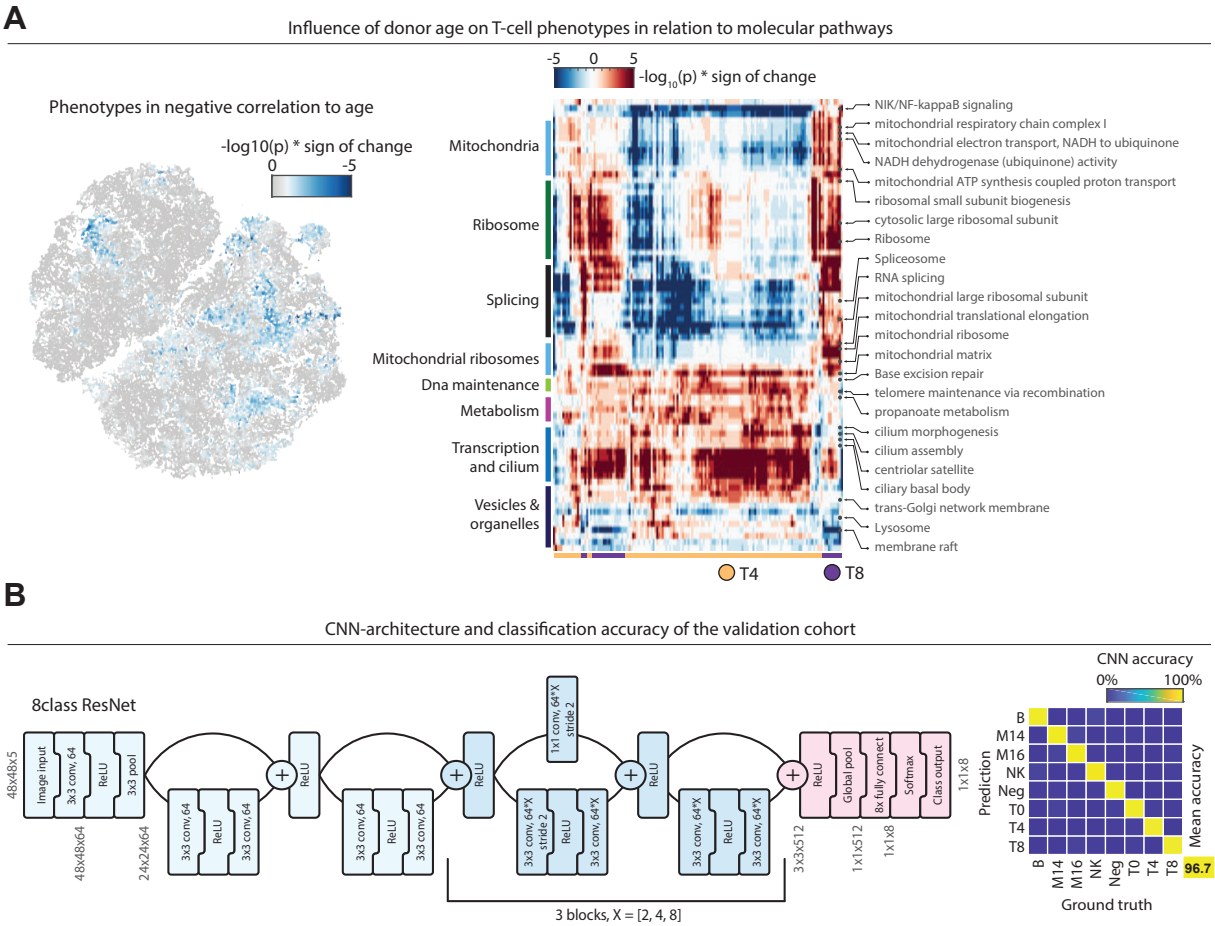
A
Influence of donor age on T-cell phenotypes in relation to molecular pathways
Phenotypes in negative correlation to age
-log10(p) * sign of change
0
-5
-5 0 5
-log10(p) * sign of change
Mitochondria
Ribosome
Splicing
Mitochondrial ribosomes
Dna maintenance
Metabolism
Transcription and cilium
Vesicles & organelles
NIK/NF-kappaB signaling
mitochondrial respiratory chain complex I
mitochondrial electron transport, NADH to ubiquinone
NADH dehydrogenase (ubiquinone) activity
mitochondrial ATP synthesis coupled proton transport
ribosomal small subunit biogenesis
cytosolic large ribosomal subunit
Ribosome
Spliceosome
RNA splicing
mitochondrial large ribosomal subunit
mitochondrial translational elongation
mitochondrial ribosome
mitochondrial matrix
Base excision repair
telomere maintenance via recombination
propanoate metabolism
cilium morphogenesis
cilium assembly
centriolar satellite
ciliary basal body
trans-Golgi network membrane
Lysosome
membrane raft
T4
T8
B
CNN-architecture and classification accuracy of the validation cohort
8class ResNet
48x48x5
Image input
3x3 conv, 64
ReLU
3x3 pool
48x48x64
24x24x64
3x3 conv, 64
ReLU
3x3 conv, 64
ReLU
1x1 conv, 64*X stride 2
3x3 conv, 64*X stride 2
3x3x512
1x1x512
1x1x8
Global pool
8x fully connect
Softmax
Class output
3 blocks, X = [2, 4, 8]
CNN accuracy
0%
100%
Prediction
Ground truth
Mean accuracy
B
M14
M16
NK
Neg
T0
T4
T8
96.7

**Figure S6. Influence of donor age on T-cell phenotypes in relation to molecular pathways.**

**(A)** Left: negative LEA associations with donor age projected onto the t-SNE (colored by $-\log_{10}(p)$). Right: Heatmap overview of all significantly enriched pathways in positive age-associated T-cells ($-\log_{10}(p)<-5$). Rows are annotations, columns are significantly age-associated cells. **(B)** Left: Schematic of the 8-class ResNet architecture used for the 15 donor validation cohort. Right: Confusion matrix of the CNN. CNN was tested on 1000 cells per class that the CNN did not see before.

**Supplementary Data File 1. Example LEA implementation.**

This zip file contains an example MATLAB implementation of a LEA analysis. The data file contains the LEA code, an example script with implementation, and the data corresponding to Figure 3 and S2, including all relevant and required annotations. The code has been tested on MATLAB version R2020b.

Supplementary Table 1

| Epitope | Vendour | Fluorophore | Clone | Host | Staining Control | Used in muliplexed | Lot |
|---|---|---|---|---|---|---|---|
| CD3 | BioLegend | Alexa Fluor 647 | UCHT1 | Mouse | 1 | yes | B246715 |
| CD4 | BioLegend | FITC | SK3 | Mouse | 1 | yes | B244280 |
| CD8 | BioLegend | Alexa Fluor 594 | RPA-T8 | Mouse | 1 | yes | B200099 |
| CD19 | BioLegend | FITC | SJ25C1 | Mouse | 3 | yes | B239447 |
| CD19 | BioLegend | PE | SJ25C1 | Mouse | 3 | yes | B237928 |
| CD56 | Beckman Coulter | PE | N901 | Mouse | 2 | yes | 52 |
| CD16 | BioLegend | PE | 3G8 | Mouse | 2 | yes | B238510 |
| CD14 | BioLegend | Alexa Fluor 647 | HCD14 | Mouse | 2&3 | yes | B260484 |
| CD11c | BioLegend | Alexa Fluor 488 | 3.9 | Mouse | 2&3 | yes | B209841 |
| CD3 | BioLegend | Alexa Fluor 488 | UCHT1 | Mouse | / | no | B278994 |
| CD4 | Biolegend | Alexa Fluor 647 | SK3 | Mouse | / | no | B293054 |
| CD8 | Biolegend | Alexa Fluor 594 | RPA-T8 | Mouse | / | no | B200099 |
| pNFkB p65 (Ser529) | eBioscience | PE | B33B4WP | Mouse | / | no | 4303324 |
| pERK1/2 (Thr202 Tyr204) | Thermo Fisher Scientific | PE | MILAN8R | Mouse | / | no | 4337535 |

**Supplementary Table 1. Staining panel details.**

Supplementary Table 2

| Compound name | Vendour | Assay conc. | Carrier solution and control |
|---|---|---|---|
| Crizotinib | Sigma-Aldrich | 10uM | 1% DMSO |
| | | 1uM | 0.1% DMSO |
| | | 0.1uM | 0.01% DMSO |
| | | 0.01uM | 0.001% DMSO |
| Dexamethasone | Sigma-Aldrich | 400ng/ml | 1% DMSO |
| | | 40ng/ml | 0.1% DMSO |
| | | 4ng/ml | 0.01% DMSO |
| | | 0.4ng/ml | 0.001% DMSO |
| Lipopolysaccharide from Escherichia coli | Sigma-Aldrich | 100ng/ml | PBS |
| | | 10ng/ml | PBS |
| | | 1ng/ml | PBS |
| | | 0.1ng/ml | PBS |
| Rituximab | Absolute antibody | 1ug/ml | PBS |
| | | 0.5ug/ml | PBS |
| | | 0.1ug/ml | PBS |
| | | 0.05ug/ml | PBS |
| Recombinant Human IL-2 | PeproTech | 100ng/ml | 0.001% (w/v) BSA in PBS |
| | | 10ng/ml | 0.0001% (w/v) BSA in PBS |
| | | 1ng/ml | 0.00001% (w/v) BSA in PBS |
| | | 0.1ng/ml | 0.000001% (w/v) BSA in PBS |
| Recombinant Human IL-4 | PeproTech | 100ng/ml | 0.001% (w/v) BSA in PBS |
| | | 10ng/ml | 0.0001% (w/v) BSA in PBS |
| | | 1ng/ml | 0.00001% (w/v) BSA in PBS |
| | | 0.1ng/ml | 0.000001% (w/v) BSA in PBS |
| Recombinant Human IL-6 | PeproTech | 100ng/ml | 0.001% (w/v) BSA in PBS |
| | | 10ng/ml | 0.0001% (w/v) BSA in PBS |
| | | 1ng/ml | 0.00001% (w/v) BSA in PBS |
| | | 0.1ng/ml | 0.000001% (w/v) BSA in PBS |
| Recombinant Human IL-10 | PeproTech | 100ng/ml | 0.001% (w/v) BSA in PBS |
| | | 10ng/ml | 0.0001% (w/v) BSA in PBS |
| | | 1ng/ml | 0.00001% (w/v) BSA in PBS |
| | | 0.1ng/ml | 0.000001% (w/v) BSA in PBS |
| Recombinant Human G-MCSF | PeproTech | 100ng/ml | 0.001% (w/v) BSA in PBS |
| | | 10ng/ml | 0.0001% (w/v) BSA in PBS |
| | | 1ng/ml | 0.00001% (w/v) BSA in PBS |
| | | 0.1ng/ml | 0.000001% (w/v) BSA in PBS |

**Supplementary Table 2. Immunomodulatory perturbations.**

Supplementary Table 3

**Discovery cohort (Figure 1, Figure 2, Figure 4, Figure 5 A-G, Figure 6 A-B)**

| Whole Blood Donor | Year of birth | Blood type | weight in kg | Height in cm | Gender | Blood pressure | Hb level |
|---|---|---|---|---|---|---|---|
| 1 | 1999 | A+ | 68 | 174 | m | 128/70 | 156 |
| 2 | 1987 | A+ | 66 | 170 | m | 173/99 | 147 |
| 3 | 1990 | A+ | 50 | 163 | f | 114/80 | 148 |
| 4 | 2000 | A+ | 63 | 168 | f | 122/74 | 133 |
| 5 | 1968 | 0- | 58 | 165 | f | 158/90 | 151 |
| 6 | 1974 | B+ | 95 | 176 | m | 156/98 | 177 |
| 7 | 1950 | 0+ | 72 | 175 | f | 126/78 | 130 |
| 8 | 1967 | A+ | 95 | 178 | m | 146/86 | 161 |
| 9 | 1967 | 0+ | 80 | 180 | m | 160/106 | 167 |
| 10 | 1965 | A+ | 80 | 180 | m | 130/82 | 167 |

**Immuno-modulatory screen (Figure 3)**

| Buffy coat donor | Year of birth | Blood type | weight in kg | Height in cm | Gender | Blood pressure | Hb level |
|---|---|---|---|---|---|---|---|
| 1 | 1968 | AB+ | 73 | 180 | m | 146/92 | 153 |

**Validation cohort (Figure 5H, Figure 6C)**

| Buffy coat Donor | Year of birth | Blood type | weight in kg | Height in cm | Gender | Blood pressure | Hb level |
|---|---|---|---|---|---|---|---|
| 1 | 1994 | B+ | 65 | 183 | m | 135/77 | 152 |
| 2 | 1970 | B+ | 69 | 177 | f | 148/92 | 147 |
| 3 | 1996 | B+ | 75 | 192 | m | 138/91 | 157 |
| 4 | 1994 | B+ | 85 | 180 | m | 124/74 | 159 |
| 5 | 1953 | B- | 65 | 178 | m | 142/95 | 168 |
| 6 | 1971 | AB- | 65 | 171 | f | 114/72 | 141 |
| 7 | 1991 | B+ | 67 | 180 | f | 135/94 | 145 |
| 8 | 1963 | B+ | 65 | 157 | f | 146/99 | 157 |
| 9 | 1963 | B+ | \ | \ | m | 170/90 | 169 |
| 10 | 1953 | 0- | 76 | 158 | f | 142/100 | 149 |
| 11 | 1999 | AB+ | 61 | 169 | f | 131/74 | 136 |
| 12 | 1960 | B+ | 90 | 182 | m | 155/98 | 151 |
| 13 | 1999 | B+ | 66 | 173 | m | 171/103 | 157 |
| 14 | 1967 | B+ | 80 | 182 | m | 162/102 | 174 |
| 15 | 1989 | AB- | 72 | 178 | f | 108/63 | 138 |

**Supplementary Table 3. Overview of the human healthy donor cohorts.**